Deghosting of towed streamer and ocean bottom cable data

Jingfeng Zhang and Arthur B. Weglein

Abstract

We present the test results of the deghosting algorithm given by Weglein et al. (2002). For the towed streamer case, when the wavelet is available, the algorithm works well as expected. When the wavelet is not available, an approximate one is obtained using the method was provided by Zhang and Weglein (2003). The deghosting algorithm still works fine using the approximate wavelet, especially when the rough duration of the source wavelet is known. For the ocean bottom case, both the source wavelet and the hydrophone measurements (P) are assumed to be known. The deghosting is performed using P and its derivative ($\frac{dP}{dz}$), which is calculated from P and the source wavelet using the triangle relationship among these three quantities (Amundsen, 1995; Weglein et al., 2002). Numerical tests of this procedure for ocean bottom case is underway.

1 Introduction

Deghosting plays an important role in seismic exploration as a pre-requisite for many data processing techniques. For the towed streamer case, although some conventional procedures may still work without deghosting, accurate deghosting is necessary for some new techniques such as imaging without velocity and non-linear inversion. For the ocean bottom case, deghosting is required even for conventional methods since the ghost notch comes very early in the spectrum. Although both the field and its derivative are measured on the ocean bottom, deghosting remains a serious problem due to for instances the coupling between the geophone and the hydrophone or the noise in the geophone data.

Last year we presented the initial test of the deghosting algorithm given by Weglein et al. (2002). The test was focused on a single frequency and an idealized model. This year we apply the deghosting algorithm to a more realistic model and the result is presented in time domain.

In the following, we will briefly review the deghosting procedure for both towed streamer and ocean bottom cases, then we will give the numerical test results followed by conclusions.

2 Theory

The deghosting formula we use is (Weglein et al., 2002):

$$P^{\text{deghosted}}(\mathbf{r},\mathbf{r}_s,\omega)=\int\limits_{M.S.}\left(P(\mathbf{r}',\mathbf{r}_s,\omega)\frac{\partial G_0^+(\mathbf{r},\mathbf{r}',\omega)}{\partial \mathbf{n}'}-G_0^+(\mathbf{r},\mathbf{r}',\omega)\frac{\partial P(\mathbf{r}',\mathbf{r}_s,\omega)}{\partial \mathbf{n}'}\right)\cdot d\mathbf{S}', \quad (1)$$

where M.S. denotes the measurement surface. In the following we will derive equation (1) and some related formulas. Start with the wave equation in the frequency domain

$$\nabla'^2 P(\mathbf{r}',\mathbf{r}_s,\omega)+\frac{\omega^2}{c^2(\mathbf{r}')}P(\mathbf{r}',\mathbf{r}_s,\omega)=A(\omega)\delta(\mathbf{r}'-\mathbf{r}_s), \quad (2)$$

where $A(\omega)$ is the source wavelet. Substituting $\frac{\omega^2}{c^2(\mathbf{r}')}$ with $\frac{\omega^2}{c_0^2}(1-\alpha(\mathbf{r}'))$, we find

$$\nabla'^2 P(\mathbf{r}',\mathbf{r}_s,\omega)+\frac{\omega^2}{c_0^2}P(\mathbf{r}',\mathbf{r}_s,\omega)=A(\omega)\delta(\mathbf{r}'-\mathbf{r}_s)+\frac{\omega^2}{c_0^2}\alpha(\mathbf{r}')P(\mathbf{r}',\mathbf{r}_s,\omega), \quad (3)$$

where $\alpha(\mathbf{r}')$ represents the difference between the actual medium and the reference medium, water. We additionally require the differential equation for Green's function in the reference medium:

$$\nabla'^2 G_0(\mathbf{r}',\mathbf{r},\omega)+\frac{\omega^2}{c_0^2}G_0(\mathbf{r}',\mathbf{r},\omega)=\delta(\mathbf{r}'-\mathbf{r}). \quad (4)$$

Of course, the Green's function G_0 for this differential equation is not unique. Its boundary conditions are versatile, and different choices lead to different applications/formulas, as we will see in a moment.

P times Equation (4) minus G_0 times Equation (3) followed by a integral on certain volume gives

$$\begin{aligned}&\int_V\left[P(\mathbf{r}',\mathbf{r}_s,\omega)\nabla'^2 G_0(\mathbf{r}',\mathbf{r},\omega)-G_0(\mathbf{r}',\mathbf{r},\omega)\nabla'^2 P(\mathbf{r}',\mathbf{r}_s,\omega)\right]d\mathbf{r}'\\ =&\int_V P(\mathbf{r}',\mathbf{r}_s,\omega)\delta(\mathbf{r}'-\mathbf{r})d\mathbf{r}'-\int_V G_0(\mathbf{r}',\mathbf{r},\omega)\left[A(\omega)\delta(\mathbf{r}'-\mathbf{r}_s)+\frac{\omega^2}{c_0^2}\alpha(\mathbf{r}')P(\mathbf{r}',\mathbf{r}_s,\omega)\right]d\mathbf{r}'.\end{aligned} \quad (5)$$

Using Green's second identity, the LHS of the equation above can be reduced to an integral on the surface of volume V:

$$\int_V\left[P(\mathbf{r}',\mathbf{r}_s,\omega)\nabla'^2 G_0(\mathbf{r}',\mathbf{r},\omega)-G_0(\mathbf{r}',\mathbf{r},\omega)\nabla'^2 P(\mathbf{r}',\mathbf{r}_s,\omega)\right]d\mathbf{r}' \quad (6)$$

$$=\oint_S\left[P(\mathbf{r}',\mathbf{r}_s,\omega)\nabla' G_0(\mathbf{r}',\mathbf{r},\omega)-G_0(\mathbf{r}',\mathbf{r},\omega)\nabla' P(\mathbf{r}',\mathbf{r}_s,\omega)\right]\cdot d\mathbf{S}'. \quad (7)$$

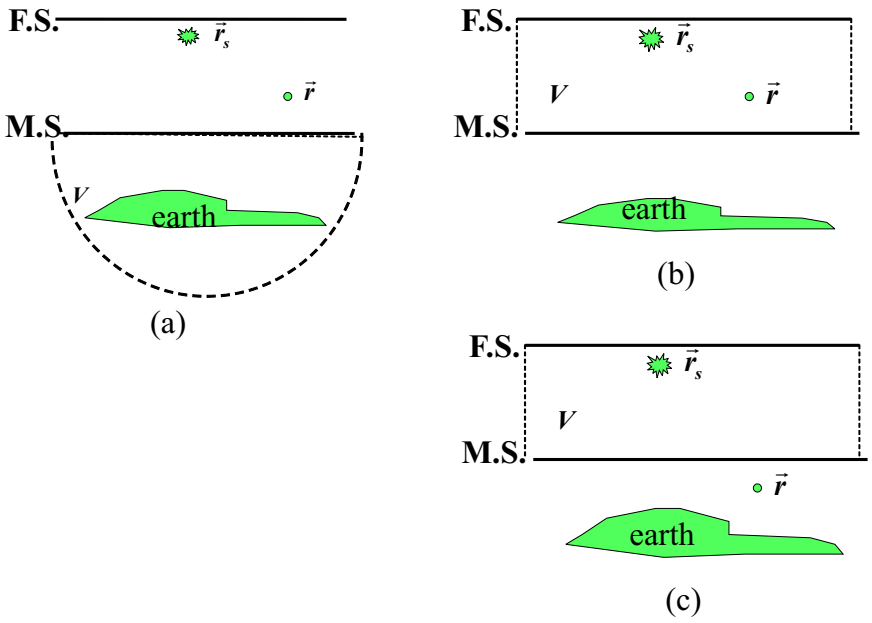

Figure 1*: Various volume configurations*

Then we have:

$$\oint_S [P(\mathbf{r}', \mathbf{r}_s, \omega)\nabla' G_0(\mathbf{r}', \mathbf{r}, \omega) - G_0(\mathbf{r}', \mathbf{r}, \omega)\nabla' P(\mathbf{r}', \mathbf{r}_s, \omega)] \cdot d\mathbf{S}'$$
$$= \int_V P(\mathbf{r}', \mathbf{r}_s, \omega)\delta(\mathbf{r}' - \mathbf{r})d\mathbf{r}' - \int_V G_0(\mathbf{r}', \mathbf{r}, \omega)\left[A(\omega)\delta(\mathbf{r}' - \mathbf{r}_s) + \frac{\omega^2}{c_0^2}\alpha(\mathbf{r}')P(\mathbf{r}', \mathbf{r}_s, \omega)\right] d\mathbf{r}'. \tag{8}$$

We will make repeated use of this formula. Choosing different volumes V, different boundary conditions for G_0 (as mentioned) and different positions $\mathbf{r}$, which can be either inside or outside volume, we can arrive at several different useful formulas.

If the whole half space below the M.S. is regarded as the volume V (Fig 1(a)), position $\mathbf{r}$ is outside V, and a causal Green's function is chosen, then we have

$$P^{deghosted}(\mathbf{r}, \mathbf{r}_s, \omega)$$
$$= \int_{M.S.} \left[P(\mathbf{r}', \mathbf{r}_s, \omega)\frac{\partial}{\partial z'}G_0^+(\mathbf{r}', \mathbf{r}, \omega) - G_0^+(\mathbf{r}', \mathbf{r}, \omega)\frac{\partial}{\partial z'}P(\mathbf{r}', \mathbf{r}_s, \omega)\right] dS'. \tag{9}$$

This is the deghosting formula we will use. Note that in the above derivation, α is regarded as $\alpha_{air}, \alpha_{water}$ and α_{earth} and only α_{earth} is inside V.

If the configuration in Fig 1(b) is used, where V horizontally extends to infinity, we have:

$$P(\mathbf{r}, \mathbf{r}_s, \omega) = A(\omega)G_0^{DD}(\mathbf{r}, \mathbf{r}_s, \omega) + \int_{M.S.} P(\mathbf{r}', \mathbf{r}_s, \omega)\frac{\partial}{\partial z'}G_0^{DD}(\mathbf{r}', \mathbf{r}, \omega)dS', \tag{10}$$

where G_0^{DD} vanishes both at the free surface (denoted as F.S.) and the M.S.. The superscript "DD" indicates the use of double Dirichlet boundary conditions. This is the field prediction formula first given by Tan (1992). It has also been used as the wavelet estimation formula by Osen et al. (1998), who claim that the wavelet of a point source can be calculated using the field measurements on the M.S. and one extra measurement between the F.S. and the M.S.

Taking the derivative with respect to z of both sides of Eq.(10) will give the derivative of the field prediction formula:

$$\frac{\partial P(\mathbf{r}, \mathbf{r}_s, \omega)}{\partial z} = A(\omega) \frac{\partial G_0^{DD}(\mathbf{r}, \mathbf{r}_s, \omega)}{\partial z} + \int\limits_{M.S.} P(\mathbf{r}', \mathbf{r}_s, \omega) \frac{\partial^2 G_0^{DD}(\mathbf{r}', \mathbf{r}, \omega)}{\partial z' \partial z} dS'. \tag{11}$$

If we choose configuration Fig 1(c) instead, the scattered field prediction formula gives

$$\begin{aligned} &\int_{M.S.} \left[P(\mathbf{r}', \mathbf{r}_s, \omega) \frac{\partial}{\partial z'} G_0^D(\mathbf{r}', \mathbf{r}, \omega) - G_0^D(\mathbf{r}', \mathbf{r}, \omega) \frac{\partial}{\partial z'} P(\mathbf{r}', \mathbf{r}_s, \omega) \right] dS' \\ &= P(\mathbf{r}, \mathbf{r}_s, \omega) - A(\omega) G_0^D(\mathbf{r}, \mathbf{r}_s, \omega) \\ &= P_s(\mathbf{r}, \mathbf{r}_s, \omega), \end{aligned} \tag{12}$$

where G_0^D is the Green's function that vanishes on the F.S.

The wavelet estimation formula (Weglein and Secrest (1990)) can be derived if the configuration of Fig 1(d) is used

$$\begin{aligned} &\int_{M.S.} \left[P(\mathbf{r}', \mathbf{r}_s, \omega) \frac{\partial}{\partial z'} G_0^D(\mathbf{r}', \mathbf{r}, \omega) - G_0^D(\mathbf{r}', \mathbf{r}, \omega) \frac{\partial}{\partial z'} P(\mathbf{r}', \mathbf{r}_s, \omega) \right] dS' \\ &= -A(\omega) G_0^D(\mathbf{r}, \mathbf{r}_s, \omega). \end{aligned} \tag{13}$$

This equation describes the triangle relationship among the source wavelet $A(\omega)$, the wave field P and its derivative $\frac{dP}{dz}$. Any one of these three quantities can be calculated if the other two are known.

As discussed in (Zhang and Weglein, 2002), deghosting can be achieved either using one measurement on two surfaces or two measurements on one surface. The issue of the difference between the deghosting formula we used and conventional up-down separation is discussed in Appendix A.

The deghosting formula Eq.(1) computes the receiver side up-going field. The same integral on the source side will get rid of the source ghost; this is discussed further in Appendix B.

2.1 Towed streamer deghosting

In Eq. (1), both P and its derivative on M.S. are needed. However, in practice, only P, the hydrophone measurement, is available. Our procedure is to use Eqs. (10) and (11) to predict the P and its derivative on a new surface between the F.S. and the M.S.. When the wavelet is available, the prediction is exact.

As pointed out by Tan (1999), G_0^{DD} in Eqs. (10) and (11) has a special property. It will vanish rapidly when the offset increases, for frequencies less than 120Hz if water speed is 1500m/s and cable depth is 6.0m. Hence for large offsets:

$$P(\mathbf{r}, \mathbf{r}_s, \omega) \approx \int\limits_{M.S.} P(\mathbf{r}', \mathbf{r}_s, \omega) \frac{\partial G_0^{DD}(\mathbf{r}', \mathbf{r}, \omega)}{\partial z'} dS' \tag{14}$$

$$\frac{\partial P(\mathbf{r}, \mathbf{r}_s, \omega)}{\partial z} \approx \int\limits_{M.S.} P(\mathbf{r}', \mathbf{r}_s, \omega) \frac{\partial^2 G_0^{DD}(\mathbf{r}', \mathbf{r}, \omega)}{\partial z' \partial z} dS' \tag{15}$$

In the absence of a wavelet estimate, we can use these approximations to perform deghosting.

Last year, we tested the deghosting algorithm both with and without the source wavelet for a single frequency and using an idealized model. It turns out that very good deghosting results may be achieved when the source wavelet is available.

However, an unsatisfactory result is produced when the approximate field and its derivative are used. Through our analysis, we found that the approximate derivative of the field is far from accurate at small offsets (Fig 2). It is clear that Eq. (15) is a good approximation for large offsets, but at small offsets results were poorer than expected. We attempted to numerically extrapolate from large to small offset, but found that small offset is not predictable due to the variability of $\frac{dP}{dz}$. We speculate that an extrapolator constrained by physics might perform better.

We found one way to successfully step into the small offset area. The idea is to approximate the wavelet so that the first rapid varying derivative of G_0^{DD} term at small offsets in Eq. (11) can be included. How to find an approximate wavelet? We went back to the wave field prediction Eq. (10), which is exact everywhere. Based on the assumption that the scattered field is small compared to the direct wave at zero offset, we assume the integral of the total field to be equal to that of the direct wave, hence neglecting the contribution of the scattered field. That is, if we put the output position $\mathbf{r}$ at zero offset, then the integral part in Eq.

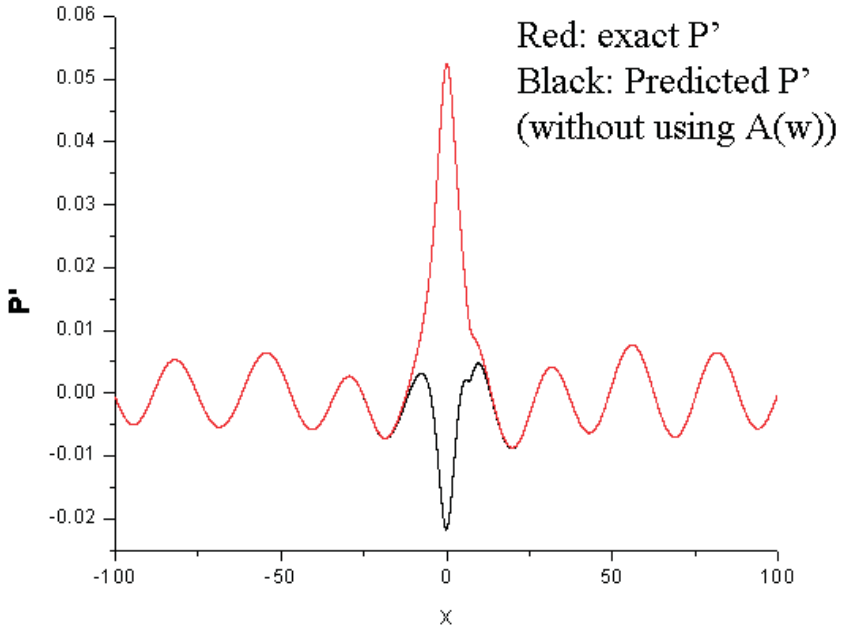

Figure 2*: The red line is the exact* $\frac{dP}{dz}$*; the black line represents the approximated* $\frac{dP}{dz}$ *without using the source wavelet*

(10) is

$$\begin{aligned}
&\int_{M.S.} P(\mathbf{r}', \mathbf{r}_s, \omega) \frac{\partial G_0^{DD}(\mathbf{r}', \mathbf{r}'', \omega)}{\partial z'} dS' \\
= &\int_{M.S.} \left[A(\omega) G_0^D(\mathbf{r}', \mathbf{r}_s, \omega) + P_s(\mathbf{r}', \mathbf{r}_s, \omega) \right] \frac{\partial G_0^{DD}(\mathbf{r}', \mathbf{r}'', \omega)}{\partial z'} dS' \\
\approx &\ A(\omega) \int_{M.S.} G_0^D(\mathbf{r}', \mathbf{r}_s, \omega) \frac{\partial G_0^{DD}(\mathbf{r}', \mathbf{r}'', \omega)}{\partial z'} dS', \qquad (16)
\end{aligned}$$

where we have neglected the integral contribution of the scattered field. Only the wavelet is unknown in the above formula, and we may approximate it this way. The wavelet approximation formula has been shown to work well in previous year's effort. Using the approximate wavelet, a much better deghosting result is achieved. That is, we achieve good deghosting results from the measurements of the wave field P on the M.S. only.

This year, instead of restricting ourselves to a single frequency, we test the last year's wavelet approximation and deghosting algorithm for all necessary frequencies and then consider the results in the time domain.

2.2 Ocean Bottom deghosting

On the ocean bottom, both the wave field P and its derivative $\frac{dP}{dz}$ are measured. In order to avoid using the measurement of the derivative of P (which is troublesome), we use P and the source wavelet to calculate it using the triangle relationship Eq. (13), as mentioned by Amundsen (1995) and Weglein et al. (2002). performing a Fourier transform with respect to x on both sides of Eq. (13), an algebraic triangle relationship is produced:

$$\begin{aligned}&\frac{\partial}{\partial z'}P(k_x, z', x_s, z_s, \omega)\\ =&\frac{A(\omega)e^{ik_x x_s}\left(e^{-ik_z z_s} - e^{ik_z z_s}\right) - ik_z P(k_x, z', x_s, z_s, \omega)\left(e^{-ik_z z'} + e^{ik_z z'}\right)}{e^{-ik_z z'} + e^{ik_z z'}},\end{aligned} \tag{17}$$

where $k_z = \sqrt{k^2 - k_x^2}$ and z' is the cable depth. The above formula is for 2D data. The 3D version is straightforward and can be found in Amundsen (1995). With P and its derivative, we can perform deghosting.

3 Numerical tests for towed streamer data

Using the Cagniard-de Hoop method, we generated the synthetic data for the following model (Fig 3): a F.S. overlies 300m of water (wave speed 1500m/s), below which is a homogeneous acoustic halfspace characterized by wave speed 2250m/s. The density is constant. The source wavelet is a Ricker wavelet with a peak frequency of 25Hz (Fig 4). The data for the towed streamer cable (at a depth of 6m) is generated.

First, we Fourier transform each trace into the frequency domain. We then process the frequencies from zero to 120Hz. Only the positive frequency is necessary to deal with, since the signal in time domain is real and hence in the Fourier domain we may assume conjugate symmetry. For each frequency, we approximate the source wavelet $A(\omega)$, predict $P(x, z, \omega)$ and its derivative at a new M.S., and deghost in frequency domain. Finally we transform the deghosted field back into the time domain.

The data generated for the towed streamer extends from 0s to 2.5s. The receiver interval is 1m and the largest receiver offset is 1500m. The seismic traces at zero offset and 1500m are presented in Fig 5. The signal includes the direct wave, the primary, multiples from first to forth order and their related ghosts.

It is apparent that the direct wave dominates at zero offset. This is the assumption upon which our wavelet approximation is based. The approximate wavelet is compared with the exact one in Fig 6 (a). There is no visible difference between the exact wavelet and the approximate one except at large t. Incidentally, if we treat the zero offset trace as the direct wave, then we can also approximate the wavelet. Fig 6(b) shows that there is almost no difference between these two methods.

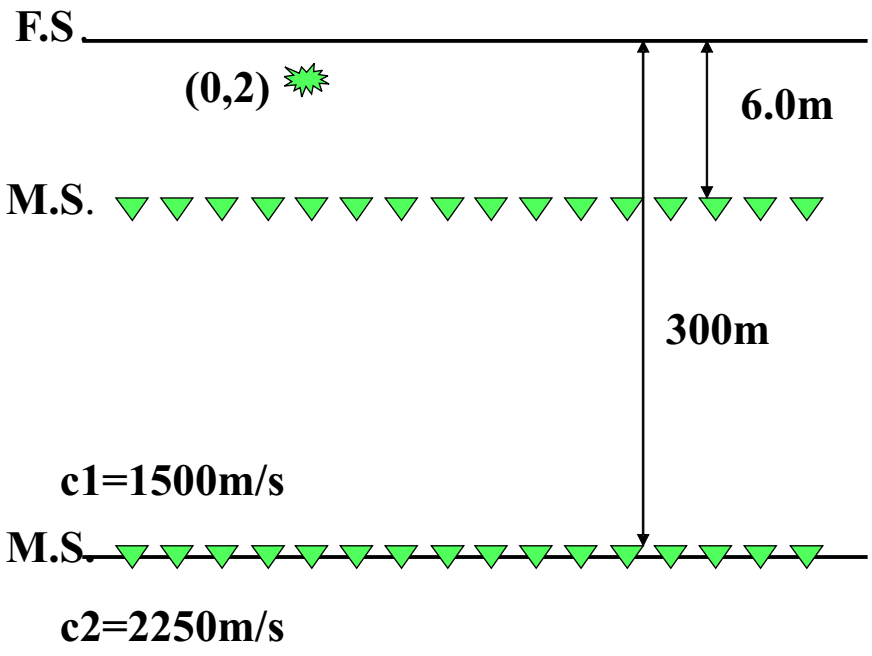

Figure 3*: Synthetic model*

With this approximate wavelet, the field and its derivative at depth z=5.9m is calculated for each frequency using Eqs. (10) and (11). The deghosting results at several offsets at a depth of z=5.8m are presented in Fig 7. The result at zero offset is poor since the approximate wavelet treats each event in the signal as part of the direct wave. This inaccurate wavelet will eventually affect each event in the deghosting result; for large offsets, it will cause new small oscillations in the signal. If the rough duration of the source wavelet is known then the late events in the approximate wavelet could be cut off and hence we could obtain the almost exact wavelet. Using the exact wavelet, the deghosting results are shown in Fig 8; even in this case, we can see that the extremely strong direct wave at zero offset has not been totally eliminated. We think this is due to numerical errors.

4 Conclusions

We test and develop the deghosting algorithm given by Weglein et al. (2002), for a towed streamer acquisition. The deghosting algorithm works well, as expected, when the source wavelet is known. Otherwise, an approximate wavelet is found to perform deghosting. The approximate wavelet could work very well if we knew the rough duration of the source wavelet.

The effectiveness of the proposed scheme is currently being tested for an ocean bottom (OBS) type acquisition.

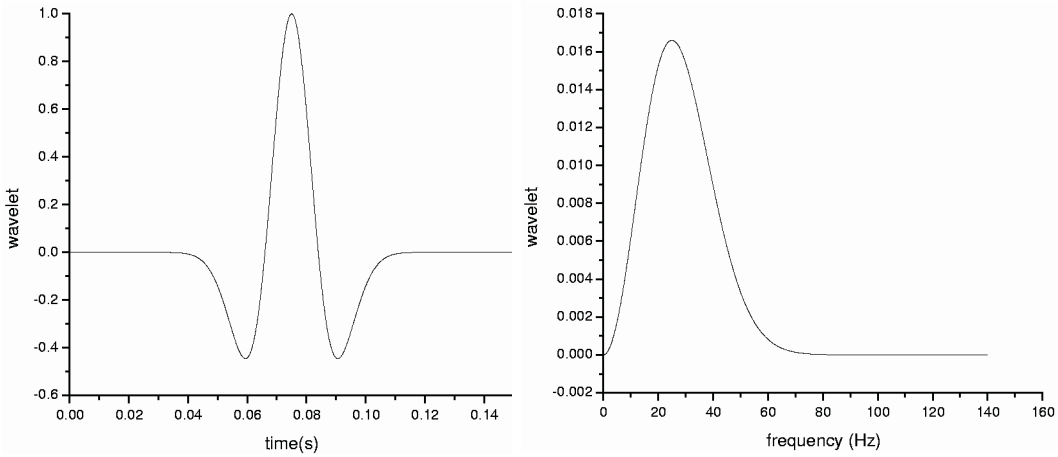

Figure 4*: Ricker wavelet with peak frequency 25Hz*

Acknowledgements

We thank Kris Innanen, Bogdan Nita, Einar Otnes, Simon Shaw, Brian Schlotmann, Adriana Ramirez, and Haiyan Zhang for their help in the preparation of the paper and valuable discussions. We are grateful to the sponsors of M-OSRP for supporting this project.

References

Amundsen, L., B.G. Secrest and B. Arntsen, 1995, Extraction of the normal component of the particle velocity from marine pressure data: Geophysics, **60**, 212-222.

Osen, A., B.G. Secrest, L. Admundsen and A. Reitan, 1998, Wavelet estimation from marine pressure measurements: Geophysics, **63**, 2108-2119.

Tan, T.H., 1992, Source signature estimation: Presented at the Internat. Conf. And Expo. of Expl. And Development Geophys., Moscow, Russia

Tan, T.H., 1999, Wavelet spectrum estimation: Geophysics, **64**, 6, 1836-1846

Weglein, A.B., and Secrest, B.G., 1990, Wavelet estimation for a multidimensional acoustic or elastic earth: Geophysics, **55**, 902-913.

Weglein, A.B., S.A. Shaw, K.H. Matson, J.L. Sheiman, R.H. Stolt, T.H. Tan, A. Osen, G.P. Correa, K.A. Innanen, Z. Guo and J. Zhang, (2002), New approaches to deghosting towed-streamer and ocean-bottom pressure measurements, 72nd SEG Annual Meeting, Salt Lake City, Utah.

Zhang, J. and Weglein, A.B., 2003, Initial tests on deghosting, M-OSRP Annual Report, **2**, p. 13-26, University of Houston.

General References

Amundsen, L., 1993, Wavenumber-based filtering of marine point source data: Geophysics, **58**, 1335-1348.

Ball, V.L. and Corrigan, D., 1996, Dual sensor summation of noisy ocean-bottom data, 66th Ann. Internat. Mtg: Soc. of Expl. Geophys., 28-31.

Barr, F.F. and Sanders, J.I., 1989, Attenuation of water column reverberations using pressure and velocity detectors in a water-bottom cable, 59th Ann. Internat. Mtg: Soc. of Expl. Geophys., 653-656.

Delima, G.R., Weglein, A.B., Porsani, M.J., and Ulrych, T.J., 1990, Robustness of a new source-signature estimation method under realistic data conditions: A deterministic-statistical approach: 60^{th} Ann. Internat. Mtg. Soc. Expl. Geophys. Expanded Abstracts, 1658-1660.

Dragoset, B., and Barr, F.J., 1994, Ocean-bottom cable dual-sensor scaling: 64^{th} Ann. Internat. Mtg. Soc. Expl. Geophys. Expanded Abstracts, 857-860.

Fokkema, J., and van den Berg, P.M., 1993, Seismic applications of acoustic reciprocity: Elsevier Science Publ.

Schneider, W.A., Larner, K.L., Burg, J.P., and Backus, M.M., 1964, A new data processing technique for the elimination of ghost arrivals on reflection seismograms: Geophysics, **29**, 5, p. 783-805.

Weglein, A.B., Tan, T.H., Shaw, S.A., Matson, K.H., Foster, D.J., 2000, Prediction of the wavefield anywhere above an ordinary towed streamer, 70^{th} Annual Meeting of the Society of Exploration Geophysicists, Calgary, Canada.

Ziolkowski, A., 1980, Source array scaling for wavelet deconvolution: Geophysical Prospecting, **28**, 902-918

Appendix A

We will show that when the prediction point $\mathbf{r}$ is brought down to the M.S., Eq. (1) gives the conventional up-down separation result. In 1D, the up-down separation is:

$$P^{up}(z', z_s, \omega) = \frac{1}{2}\left[P(z', z_s, \omega) - \frac{1}{ik}\frac{dP(z', z_s, \omega)}{dz'}\right]. \tag{18}$$

The deghosting formula in Eq. (1) reduces to

$$P^{up}(z, z_s, \omega) = P(z', z_s, \omega)\frac{dG^+(z, z', \omega)}{dz'} - G^+(z, z', \omega)\frac{dP(z', z_s, \omega)}{dz'}, \tag{19}$$

where, assuming $z' > z > z_s > 0$,

$$G^+(z, z', \omega) = \frac{1}{2ik}e^{ik(z-z')},$$
$$\frac{dG^+(z, z', \omega)}{dz'} = \frac{1}{2}e^{ik(z-z')}.$$

At the limit $z \to z'$,

$$G^+(z, z', \omega) = \frac{1}{2ik},$$
$$\frac{dG^+(z, z', \omega)}{dz'} = \frac{1}{2},$$

so

$$P^{up}(z', z_s, \omega) = \frac{1}{2}\left[P(z', z_s, \omega) - \frac{1}{ik}\frac{dP(z', z_s, \omega)}{dz'}\right],$$

which is Eq. (18) as desired.

Appendix B

Here we show that the integral in Eq. (1), if carried out on the source side, will eliminate the source ghosts. If we switch the source and receiver positions in Fig 9 the same data would be recorded (see Eq. 2). The many-source experiment in Fig 10 will therefore produce the same results as that of Fig 11.

The source-side deghosting of Fig 10 is exactly the receiver-side deghosting of Fig 11 (i.e., the source ghosts of Fig 10 would be the receiver ghosts of Fig 11). So the source-side deghosting seen in Fig 10 is

$$P^{\text{source deghosted}}(\mathbf{r}'_s, \mathbf{r}_g, \omega) = \int\limits_{S.S.} \left(P(\mathbf{r}_s, \mathbf{r}_g, \omega)\frac{\partial G_0^+(\mathbf{r}_s, \mathbf{r}'_s, \omega)}{\partial \mathbf{n}} - G_0^+(\mathbf{r}_s, \mathbf{r}'_s, \omega)\frac{\partial P(\mathbf{r}_g, \mathbf{r}_s, \omega)}{\partial \mathbf{n}}\right) \cdot d\mathbf{S}, \tag{20}$$

where S.S. represents the source surface and $\mathbf{r}'_s$ can be any point between the S.S. and the F.S. The formula above computes the source-side deghosted field measured at $\mathbf{r}_g$ due to source at $\mathbf{r}'_s$; the latter may be brought down to $\mathbf{r}_s$ in Fig 9 in accordance with the results of Appendix A.

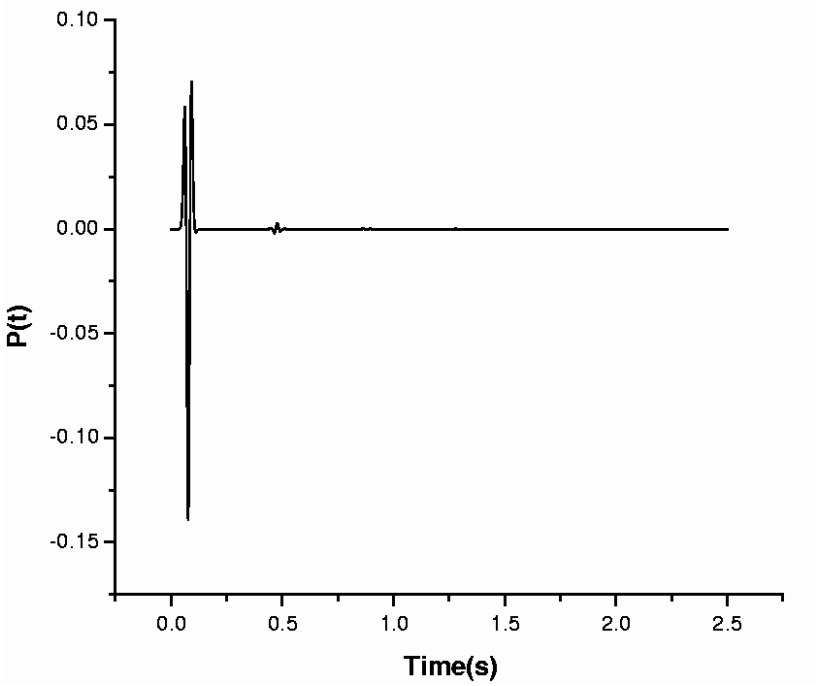

(a)

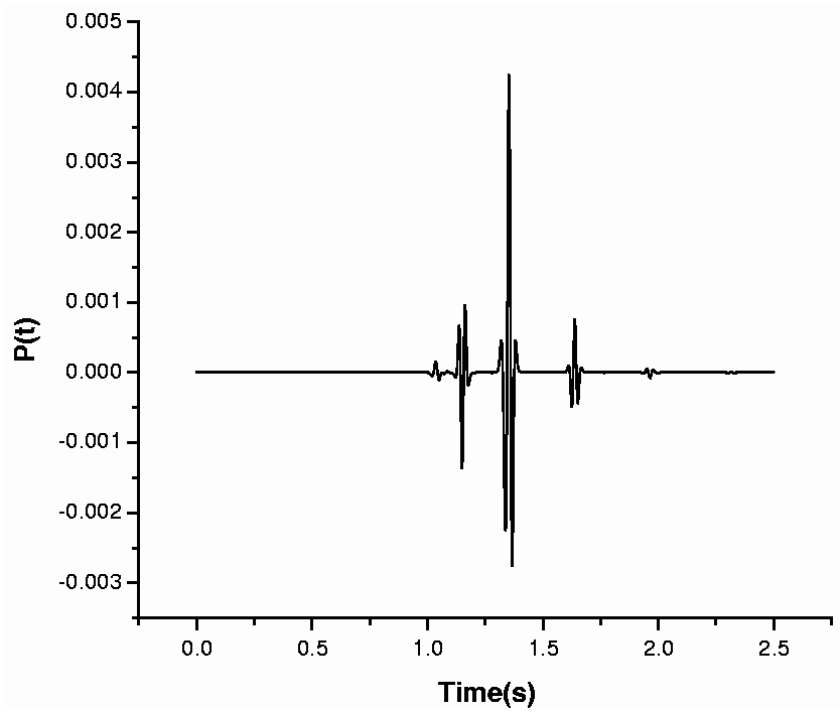

(b)

Figure 5*: (a) Data received at (0,6.0). (b) Data received at (1500,6.0)*

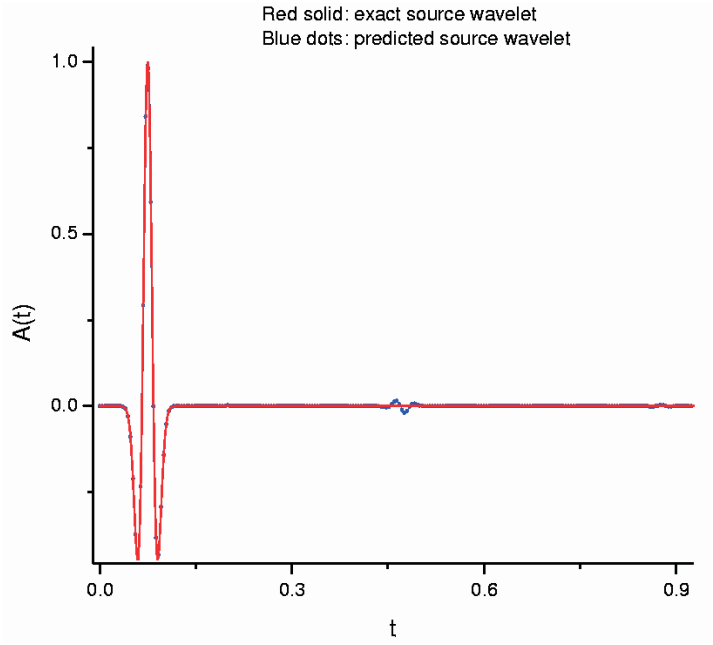

(a)

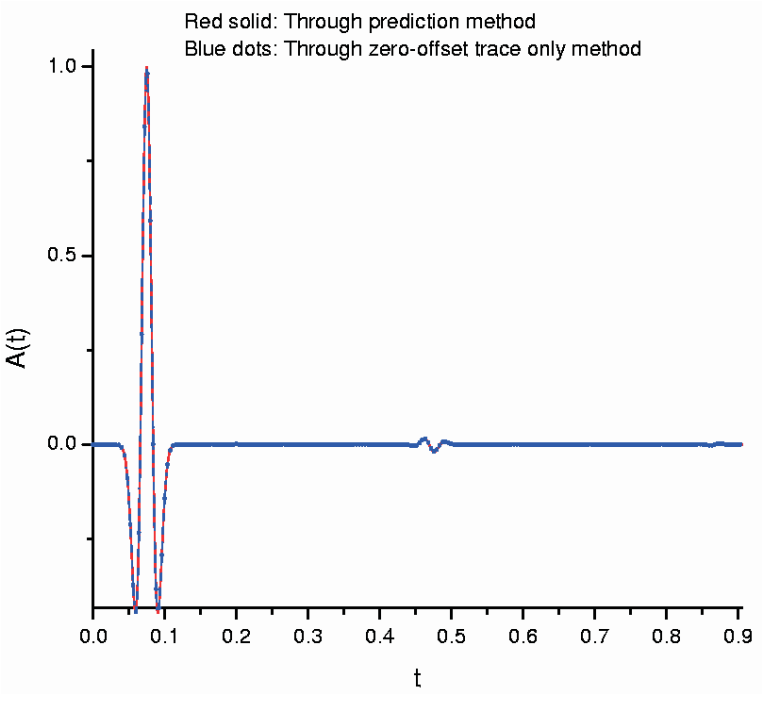

(b)

Figure 6: *(a) Red solid: exact source wavelet. Blue dots: approximated source wavelet using equation (16). (b) Red solid: wavelet using equation (16), approximate source. Blue dots: Approximate source wavelet using zero trace only.*

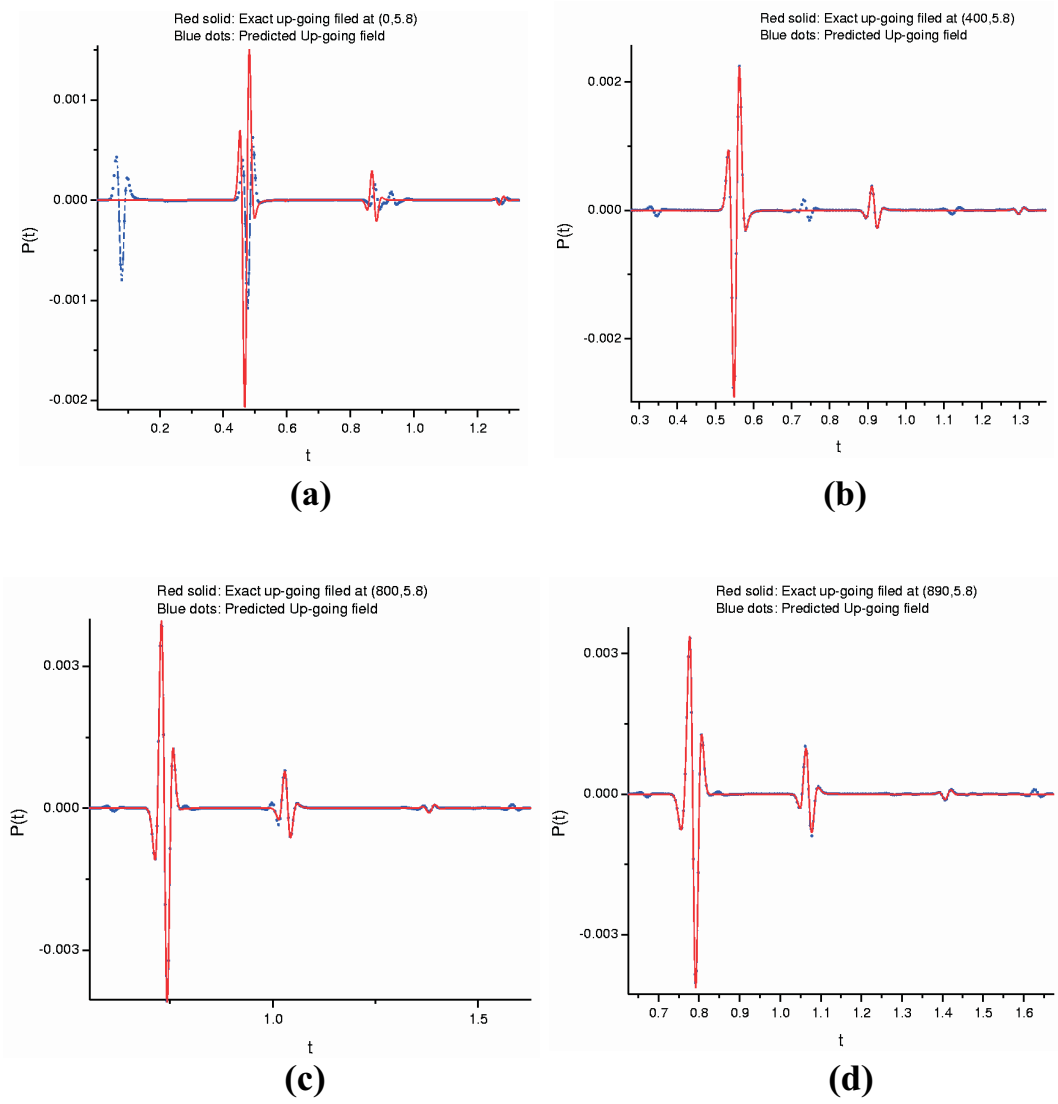

Figure 7: *Red solid: exact up-going field. Blue dots: predicted up-going field using approximate source wavelet. (a) At (0,5.8). (b) At (400,5.8). (c) At (800,5.8). (d) At (890,5.8).*

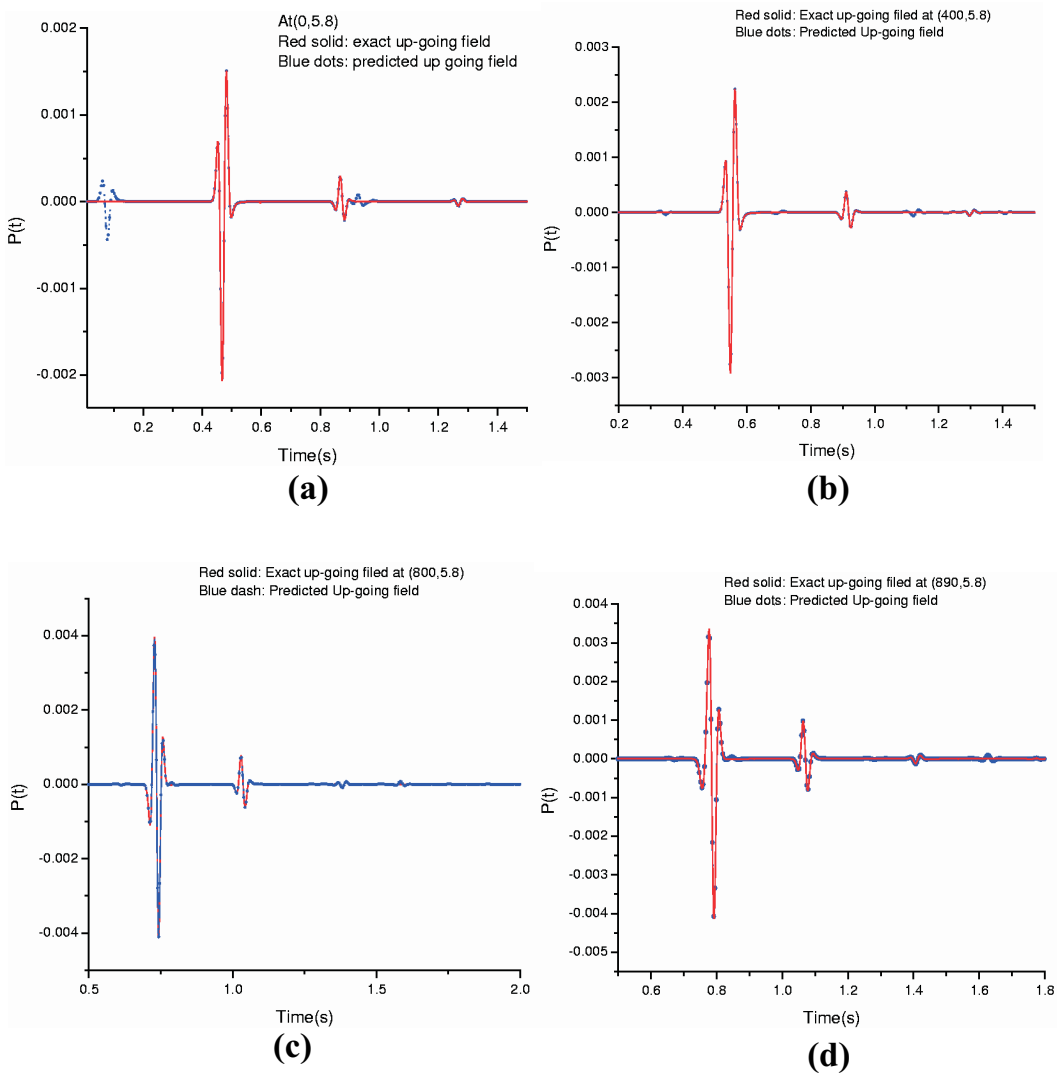

Figure 8: *(Red solid: exact up-going field. Blue dots: predicted up-going field using approximate source wavelet. (a) At (0,5.8). (b) At (400,5.8). (c) At (800,5.8). (d) At (890,5.8)*

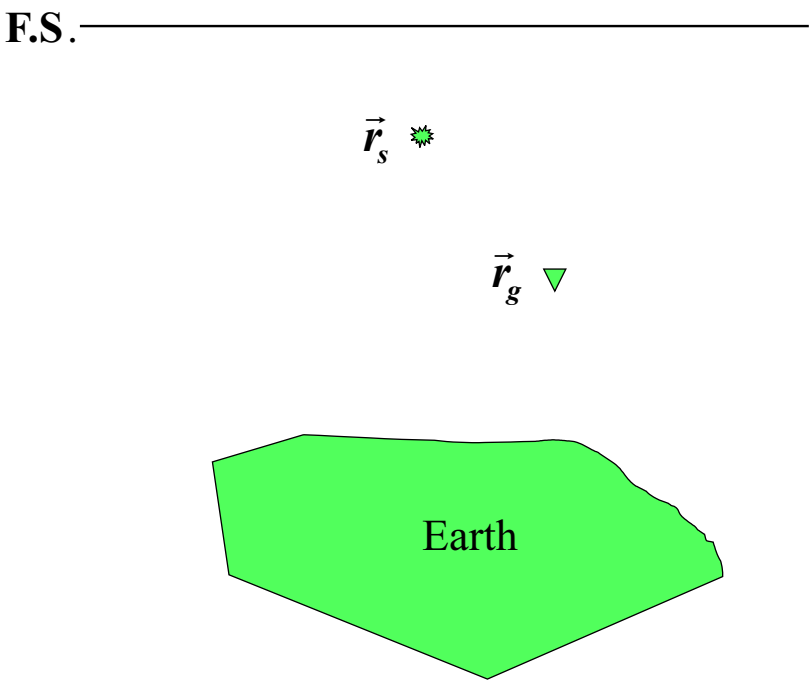

Figure 9*: Single point source and point receiver experiment*

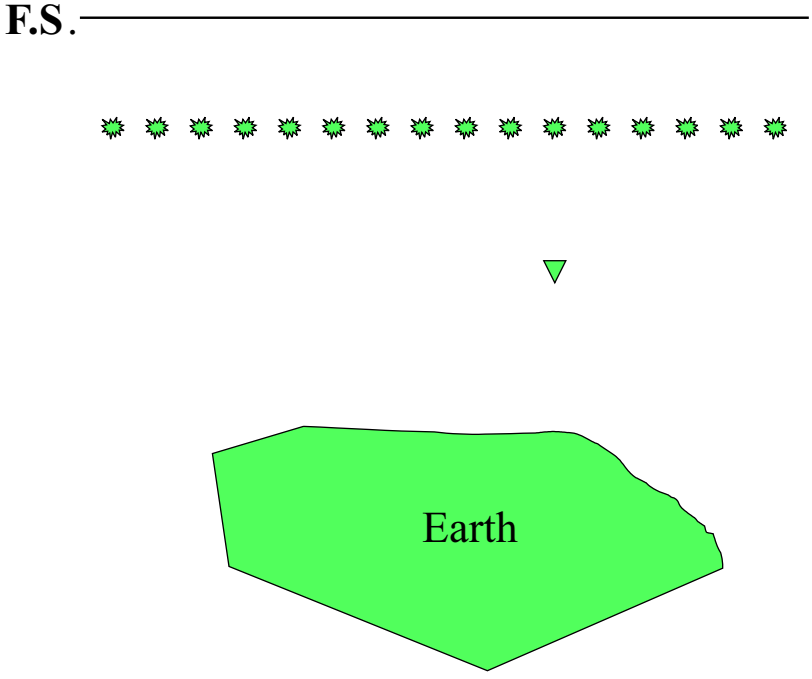

Figure 10*: Many source experiment*

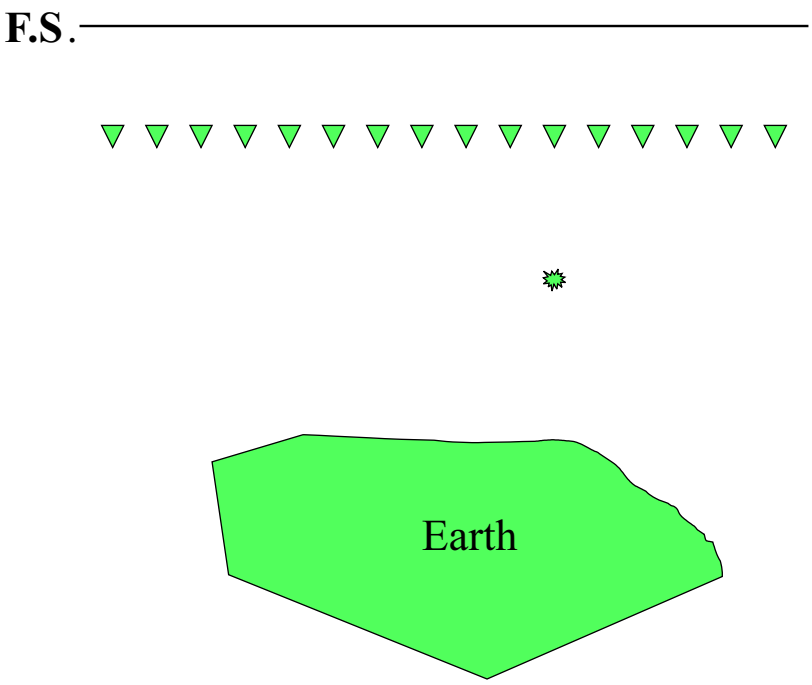

Figure 11*: Single source experiment with an array of receivers.*